Modelling and Control of a Quad-Rotor Robot

Paul Pounds, Robert Mahony, Peter Corke
Australian National University, Canberra, Australia
CSIRO ICT Centre, Brisbane, Australia
paul.pounds@anu.edu.au, mahony@ieee.org, peter.corke@csiro.au

Abstract

To date, most quad-rotor aerial robots have been based on flying toys. Although such systems can be used as prototypes, they are not sufficiently robust to serve as experimental robotics platforms. We have developed the X-4 Flyer, a quad-rotor robot using custom-built chassis and avionics with off-the-shelf motors and batteries, to be a highly reliable experimental platform. The vehicle uses tuned plant dynamics with an onboard embedded attitude controller to stabilise flight. A linear SISO controller was designed to regulate flyer attitude.

1 Introduction

A major limitation of helicopters is the need for extensive, and costly, maintenance for reliable flight. Unmanned Air Vehicles (UAVs) and Micro Air Vehicle (MAV) rotorcraft are no exception. Simplifying the mechanical structure of a flying machine produces clear benefits for the logistics of operating these devices.

Quad-rotors are robust and simple helicopters as they do not have the complicated swashplates and linkages found in conventional rotorcraft. The majority of four-rotor aerobots are constructed from remote-control toy components. As a result, these craft lack the necessary reliability and performance to be practical experimental platforms.

1.1 Existing Quad-Rotor Platforms

Several quad-rotor craft have been developed recently, for use as a toy or for research. Many research quad-rotors began life as a commercially available toy, such as the HMX-4 and RCtoys' Draganflyer. Unmodified, these craft typically consist of light airframes with plastic rotors. They are powered by NiCd or Li-Poly cells and use rate feedback from MEMS gyros. These quad-rotors generally have no attitude stability.

Research quad-rotors add automatic stability and use a variety of hardware and control schemes. CSIRO's quad-rotor flyer, for example, is a Draganflyer derivative that uses visual servoing and an Inertial Measurement Unit (IMU) to stabilise the craft over a blob target. Other quad-rotors include Eidgenossische Technische Hochschule Zurich's 'OS4' [Bouabdallah *et al*, 2004], a belt-driven flyer with low-aspect ratio blades; CEA's 'X4-flyer'[1], a small quad-rotor with four blades per motor [Guenard *et al*, 2005]; and Cornell's Autonomous Flying Vehicle, a large craft using hobby aeroplane propellers.

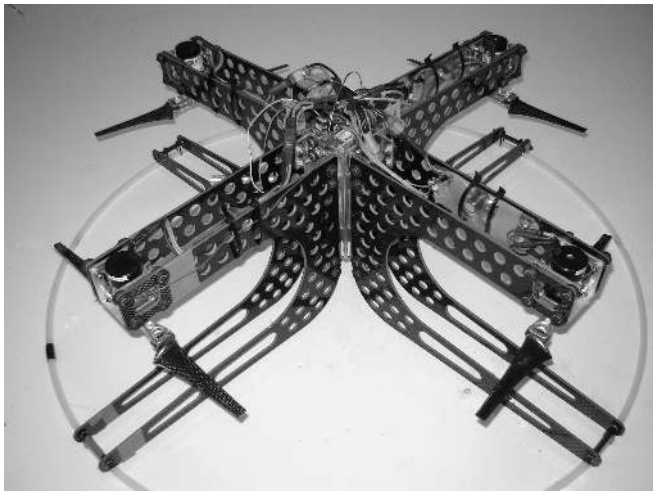

Figure 1: X-4 Flyer Mark II.

The Australian National University's (ANU) X-4 Flyer quad-rotor MAV (cf. Fig. 1) aims to address the problems faced by small-scale UAVs. The X-4 is much heavier than similar robots: it weighs 4 kg total and is designed to carry a 1 kg payload. It has a strong carbon-fibre and aluminium chassis and a high thrust-to-weight ratio. The motors and cells used are off-the-shelf components. The motors directly drive the rotors, eliminating the need for a gearbox – the robot has only eight moving

1. Although similarly named, the ANU X-4 Flyer and CEA X4-flyer are quite different craft

parts. As a result, the flyer is rugged and reliable with little scope for catastrophic failure in flight. It promises a practical payload capacity with a substantial flight duration.

1.2 Goals of Current Development

High-performance rotors and speed controllers have been developed for the X-4 Flyer. These have adequately solved the problems of thrust generation and dynamic motor speed performance [Pounds *et al*, 2005], [Pounds *et al*, 2007]. In addition, a model of the flight dynamics, including rotor flapping effects, was derived. A 3D simulator of the craft generated state trajectories of the robot for a variety of configurations, subjected to disturbances.

Current work on the flyer aims to stabilise the aircraft in roll, pitch and yaw. Continuous flight requires the pitch and roll angles to remain around zero, except when actively translating. The natural instability of flying systems requires active compensation. The special design for the chassis results in purely divergent instability in pitch and roll that a controller can readily correct.

In this paper we present the X-4 Flyer as a fully-functional aerial robot. The dynamics of quad-rotor helicopters with blade flapping are studied. We estimate the system parameters from data to produce a numerical plant model. Based on a 6DOF aerodynamic model we derive decoupled dynamics in longitudinal (pitch/roll) and azimuthal modes. The control approach is to optimise the mechanical design for control of these dynamics and implement linear SISO control in the decoupled dynamics. We describe the controller used to stabilise the craft in simulation and then go on to demonstrate the function of the roll and pitch compensation in tethered flight.

2 X-4 Hardware and Construction

The X-4 Flyer is set apart from other quad-rotor vehicles by its larger construction. It consists of a chassis, motors and power cells, and attitude control and communications avionics. Each subsystem is described in detail below:

2.1 Chassis

The X-4 has an aluminium centre frame with carbon fibre-foam sandwich arms. Regularly spaced mounting points allows the CoG to be shifted easily. Motors and batteries are mounted as far from the central axis as possible. The arms angle down slightly to provide more clearance between the bottom of the arms and flapping rotor tips. The rotor mounts are teetering hubs, a freely pivoting joint between the drive shafts and rotor blades, machined from aluminium. The blades are screw-clamped between the rotor mount top and bottom plates.

2.2 Drive System

The X-4's rotors are designed to lift the flyer with an additional 30 per cent control margin (greater than 5.2 kg). The blades are three-ply carbon fibre and were designed and fabricated at the ANU. The geometry is designed so that the rotor tips flex to the optimal operating angle under load. The ANUX2 airfoil used is a custom section made specially for the rotors.

The rotors are driven by Jeti Phasor 30-3 three-phase brushless motors for radio-controlled aircraft. They offer high torque performance that allows for direct drive of the rotors, eliminating the need for gearing. The motors can pass more than 300 W and are rated up to 35 A.

Custom motor control boards commutate the motors. These were developed by the CSIRO Queensland Centre for Advanced Technology ICT group. The boards are based around the Freescale HC12D60A microprocessor and Toshiba TB9060 brushless motor speed control chip.

Power is provided by 24 Li-Poly 2000 mA·h high-discharge cells. Each cell has a nominal voltage of 3.7 V, ranging from 4.2 V fully charged and dropping to 3 V at depletion. Each cell can deliver up to 20 A. The batteries are connected to a power bus of six parallel sets of four cells in series; that is, 14.8 V nominal voltage and 120 A of current draw per motor. This gives the flyer an expected flight time of 11 minutes at hover speed.

2.3 Control

The craft is stabilised by an onboard embedded HC12 controller. The controller reads attitude from a CSIRO Eimu IMU that provides angular rate and acceleration measurements and angular position estimates at 50 Hz. The controller outputs rotor speed references to the motor control cards over the CANbus, also at 50 Hz.

2.4 Command and Telemetry

Human directions to the robot and information about the X-4's state are transmitted over a long-range Bluetooth serial module connected to a laptop base station running Linux. The Bluetooth unit has a range of up to 100 m. Telemetry from the flyer is logged by the base station and displayed on-screen. The user can issue commands via the laptop using the keyboard and a JR-X3810 radio handset.

The radio handset can also trigger a safety kill switch on the X-4, independently of the Bluetooth communications channel, using an onboard radio receiver. In an emergency the kill switch can stop the rotors instantly by disabling the motor control boards, even if data communications is lost.

3 Quad-Rotor Dynamics

The dynamic model described in [Pounds *et al*, 2004] added articulated flapping rotors to the basic quad-rotor

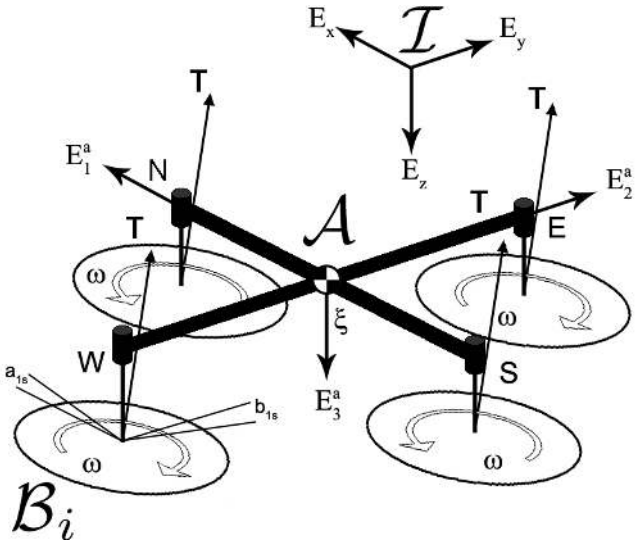

Figure 2: Flapping Quad-Rotor Free-body Diagram.

rigid body dynamics model. The current configuration of the X-4 Flyer does not incorporate the hub-springs originally included in the model. As a result, the flapping equations can be substantially simplified:

The right-hand inertial frame is denoted by $\mathcal{I}=\{E_x, E_y, E_z\}$, where x is aligned with the front of the craft and z is in the direction of gravity, and $\xi = (x, y, z)$ is the origin of the body fixed frame $\mathcal{A}=\{E_1^a, E_2^a, E_3^a\}$. The frame $\mathcal{A}$ is related to $\mathcal{I}$ by the rotation matrix $R : \mathcal{A} \rightarrow \mathcal{I}$. V and Ω are the linear and angular velocities of the frame in $\mathcal{A}$ (cf. Fig. 2).

The equations are:

$$\dot{\xi} = RV \quad (1)$$

$$m\dot{V} = -m\Omega \times V + mgR^{\mathrm{T}}e_3 + \sum_{N,S,E,W} T_i \quad (2)$$

$$\dot{R} = R \cdot \mathrm{sk}(\Omega) \quad (3)$$

$$\mathrm{I}\dot{\Omega} = -\Omega \times \mathrm{I}\Omega + \sum_{N,S,E,W} [Q_i + M_i] \quad (4)$$

$$T_i = C_{\mathrm{T}}\rho A r^2 \omega_i^2 \begin{pmatrix} -s_{a_{1s}i} \\ c_{a_{1s}i}s_{b_{1s}i} \\ c_{b_{1s}i}c_{a_{1s}i} \end{pmatrix} \quad (5)$$

$$Q_i = C_{\mathrm{Q}}\rho A r^3 \omega_i |\omega_i| e_3 \quad (6)$$

$$M_i = T_i \times D_i \quad (7)$$

where m and I are the mass and rotational inertia of the flyer, g is acceleration due to gravity, rho is the density of air, r is the rotor radius, and A is the rotor disc area. In equation 6, ω is multiplied by its magnitude to preserve the sign of rotation for counter-rotating rotors.

Here $\mathrm{sk}(x)$ is the skew-symmetric matrix such that $\mathrm{sk}(a)b = a \times b$ for vectors in $\Re^3$. The s_x and c_x notations represent $\sin x$ and $\cos x$ respectively. The rotation matrix R is constructed with the yaw-pitch-roll, $\eta = (\phi, \theta, \psi)$ Euler angles. Rotors are indexed by their corresponding compass directions: North, South, East and West ($NSEW$), where N indicates the front rotor. Correspondingly, D_i is the rotor displacement from the flyer centre of mass:

$$D_N = \begin{pmatrix} 0 & d & h \end{pmatrix} \quad (8)$$

$$D_S = \begin{pmatrix} 0 & -d & h \end{pmatrix} \quad (9)$$

$$D_E = \begin{pmatrix} d & 0 & h \end{pmatrix} \quad (10)$$

$$D_W = \begin{pmatrix} -d & 0 & h \end{pmatrix} \quad (11)$$

where d is the arm length of the flyer and h is the height of the rotors above the CoG.

Vectors T_i and Q_i are the rotor thrust and torque, and M_i is the moment due to the thrust vector of the ith rotor – for a teetering rotor, the moment produced by the rotor flapping is due solely to the thrust vector acting around a displacement from the vehicle's centre of gravity. The first harmonic of the longitudinal and lateral flapping angles of the ith rotor are denoted by a_{1s_i} and b_{1s_i}. The non-dimensionalised thrust and torque coefficients, C_{T} and C_{Q}, are treated as constants here. The speed of the ith rotor is given by ω_i. The non-dimensionalised thrust coefficient and flapping equations are discussed in more detail in Sections 3.1 and 3.2.

3.1 Pitch and Roll Rotor Damping

A quad-rotor necessarily has a horizontal displacement between its masts and CoG. When the craft rolls and pitches, the rotors experience a vertical velocity, leading to a change in the inflow angle. From Prouty [Prouty, 2002, pp 101], C_{T} can be related to the vertical velocity, V_c, by:

$$C_{\mathrm{T}}/\sigma = \frac{a(\alpha)}{4}\left[\theta_{\mathrm{tip}} - \frac{v_i + V_c}{\omega r}\right] \quad (12)$$

where a is the polar lift slope, $theta_{\mathrm{tip}}$ is the geometric blade angle at the tip of the rotor, v_i is the induced velocity through the rotor, and σ is the solidity of the disc - the ratio of the surface area of the blades and the rotor disc area.

The polar lift slope is itself a function of the rotor blade angle of attack, α. It is highly nonlinear for some airfoils and so the relation can be better expressed as a variation around a set point, C_{T0}:

$$C_{\mathrm{T}i} = C_{\mathrm{T0}} + \Delta C_{\mathrm{T}i} \quad (13)$$

where ΔC_{T} is the change induced by the changing inflow conditions. From Equation 12, this is written as:

$$\Delta C_{\mathrm{T}i} = -\frac{a_0}{4}\frac{\sigma}{\omega_i r}(V + \Omega \times D_i)e_3 \quad (14)$$

where a_0 is the lift slope at the set point.

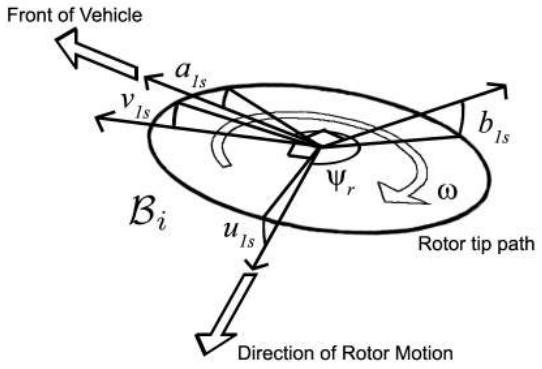

Figure 3: Blade Flapping Angle Rotation.

3.2 Blade Flapping

When the rotors translate horizontally there is a difference in blade lift between the advancing and retreating blades, which causes the rotor tip path plane to tilt. The resulting angle of the rotor plane is obtained by simultaneously solving the constant and sinusoidal components of the blade centrifugal-aerodynamic-static weight moment system. Flapping is important, as previous simulations of the X-4 have shown that the tilting rotor can introduce significant stability effects for the vehicle [Pounds *et al*, 2004].

The dynamics of rotor flapping are very fast, occurring within one revolution of the rotor [Leishman, 2006], compared to the rigid body dynamics of the helicopter. Consequently, the blade flapping equations can be written as instantaneous functions of the craft's planar velocity.

A quad-rotor's flight is not limited to longitudinal motion – when the vehicle moves arbitrarily, the flapping motions of the rotors need not be in line with the nominal front of the aircraft. When the craft yaws the linear velocity of the rotor hubs about e_3 is added to the motion of the vehicle.

The flapping of the ith rotor due to planar motion is found by calculating the magnitude and direction of rotor's translation and defining a local frame of reference, $\mathcal{B}_i$, aligned in that direction. We calculate the longitudinal and lateral flapping angles in the rotor frame ($u_{1_s i}$ and $v_{1_s i}$) and then re-express them in the body-fixed frame ($a_{1_s i}$ and $b_{1_s i}$ using a rotation matrix (cf. Fig. 3). This allows us to avoid computational complexity by using standard flapping equations in the local frame.

The per-rotor flapping is found by first computing the advance ratio and azimuthal direction of the rotor. We derive this as:

$$V_{ri} = V + \Omega \times D_i \tag{15}$$

$$\mu_{ri} = \frac{\|V_{r(1,2)i}\|}{\omega_i R} \tag{16}$$

$$\psi_{ri} = \arctan\left(\frac{V_{r(2)i}}{V_{r(1)i}}\right) \tag{17}$$

where $V_{r(n)i}$ is the nth element of the ith rotor's velocity vector, μ_{ri} is the ith rotor's advance ratio and ψ_{ri} is the azimuthal direction of motion.

The configuration of the X-4 Flyer dispenses with the sprung virtual hinge offsets used previously. Thus, the equations describing this motion can be greatly simplified: the longitudinal and lateral flapping angle solutions of the ith rotor in the local frame, $\mathcal{B}_i$, are:

$$u_{1_s i} = \frac{1}{1 - \frac{\mu_{ri}^2}{2}} \mu_{ri} \left(4\theta_t - 2\lambda_i\right) \tag{18}$$

$$v_{1_s i} = \frac{1}{1 + \frac{\mu_{ri}^2}{2}} \frac{4}{3} \left(\frac{C_\mathrm{T}}{\sigma} \frac{2}{3} \frac{\mu_{ri}\gamma}{a} + \mu_{ri}\right) \tag{19}$$

respectively, where λ_i is the non-dimensionalised inflow of the ith rotor, approximated by

$$\lambda_i = \sqrt{C_\mathrm{T}/2} \tag{20}$$

and γ is the Lock Number [Leishman, 2006]:

$$\gamma = \frac{\rho a_0 c r^4}{\mathrm{I}_b} \tag{21}$$

where $\mathrm{I_b}$ is the rotational inertia of the blade about the flapping hinge.

These are transformed back into the body-fixed frame by the frame mapping between $\mathcal{A}$ and $\mathcal{B}_i$, J_i to derive the body-frame flapping angles due to motion of the flyer:

$${}^{\mathcal{A}}J_{\mathcal{B}_i} = \begin{pmatrix} \cos\psi_{ri} & -\sin\psi_{ri} \\ \sin\psi_{ri} & \cos\psi_{ri} \end{pmatrix} \tag{22}$$

$$\begin{pmatrix} a_{1_s i} \\ b_{1_s i} \end{pmatrix} = {}^{\mathcal{A}}J_{\mathcal{B}_i} \begin{pmatrix} u_{1_s i} \\ v_{1_s i} \end{pmatrix} \tag{23}$$

The components of the flapping angles produced by the craft's pitch and roll rates [Prouty, 2002] are added to those of the body-fixed frame:

$$a_{1_s i} = \ldots + \frac{-\frac{16}{\gamma}\left(\frac{q}{\omega}\right) + \left(\frac{p}{\omega}\right)}{1 - \frac{\mu_i^2}{2}} \tag{24}$$

$$b_{1_s i} = \ldots + \frac{-\frac{16}{\gamma}\left(\frac{p}{\omega}\right) + \left(\frac{p}{\omega}\right)}{1 - \frac{\mu_i^2}{2}} \tag{25}$$

	Value	Error	Unit
a_0	5.5	± 0.5	
c_{tip}	0.012	± 0.001	m
m	4.34	$\pm 5 \times 10^{-3}$	kg
A	0.0855	$\pm 0.1 \times 10^{-3}$	m^2
C_T	0.0047	$\pm 0.2 \times 10^{-3}$	
C_Q	0.228×10^{-3}	$\pm 0.015 \times 10^{-3}$	
I_b	40.887×10^{-6}	$\pm 3.655 \times 10^{-6}$	kg·m^2
R	0.165	$\pm 0.5 \times 10^{-3}$	m
ρ	1.184	Not available	kg·m^{-3}
γ	1.417	± 0.133	
λ	0.049	$\pm 2 \times 10^{-3}$	
θ_{tip}	4.4	± 0.5	deg
σ	0.054	$\pm 1 \times 10^{-3}$	
ω_{hover}	850	± 5	rad·s^{-1}

Table 1: Aerodynamic Parameters and Associated Error.

4 Model Parameterisation and Stability

Designing a controller based on this model requires parameters of the physical system to be specified. Most of these values are dictated by the flight performance of the system; some, most importantly h, can be chosen freely. The error associated with each parameter defines the envelope of the plant model's dynamic response. We analyse the system behaviour within this envelope to determine the best value of h, the height of the rotor plane above the CoG.

4.1 Measured Values and Uncertainty

We have a set of parameter estimates, taken directly from measurements or derived from experiments, along with the associated error. In the case of parameters computed from other known values, the associated error was also computed:

- Aerodynamic parameters
  Rotor, blade and aerodynamic parameters are obtained through measurement, computation, simulation or from references. These are listed in Table 1.
- Masses and Displacements
  Component masses and distances measured with respect to the rotor plane, (masses ± 0.005 kg, distances ± 0.005 m) are given in Table 2. Note that this table is not a complete listing of all masses, but includes all major masses – screws and fasteners are omitted (cf. Fig. 4).
- Rotational Inertia Computed from the previous values by treating the masses as point masses, the diagonal entries of the inertial matrix are given in Table 3. The CoG is 0.0071 ± 0.005 m above the rotor plane.

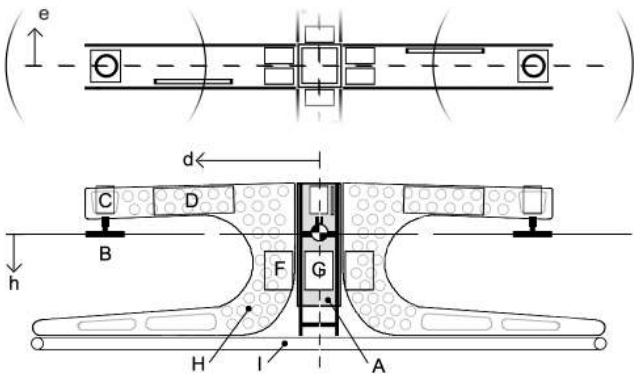

Figure 4: X-4 Component Offsets.

	Part	mass/kg	d/m	e/m	h/m
A	Avionics	0.242	0	0	-0.02
B	Rotor	0.046	0.315	0	0
C	Motor	0.288	0.315	0	-0.06
D	ESC	0.074	0.15	0.035	-0.055
E	Powerbus	0.099	0	0	-0.13
F	$\text{Batt}_{\text{long}}$	0.165	0.0125	0.06	0.035
G	Batt_{lat}	0.165	0.0	0.04	0.035
H	Arm	0.039	0.157	0.035	0.04
I	Hoop	0.200	0	0	-0.17

Table 2: Component Masses and Offsets.

4.2 Unforced Stability Analysis

The dominant dynamics of a helicopter, or a quad-rotor, are associated with the longitudinal dynamics of the vehicle. Around hover, the motion of a helicopter is largely decoupled in each axis. The symmetry of quad-rotors means that the important attitude dynamics can be described by a single equation. We analyse the natural stability of these dynamics to provide insight into the best airframe geometry for controllability of the system.

In earlier work [Pounds *et al*, 2004], we applied Prouty's stability derivation to analyse the near-hover dynamics of quad-rotors. This treatment furthers that analysis through the addition of terms specific to quad-rotors and the elimination of flapping due to hub springs that are not used in the current X-4 Flyer.

From the basic dynamic equations for a helicopter constrained to translate in x and rotate in pitch only without

	Value	Error	Unit
I_{XX}	0.0820	± 0.0025	kg·m^2
I_{YY}	0.0845	± 0.0029	kg·m^2
I_{ZZ}	0.1377	± 0.0059	kg·m^2

Table 3: Diagonal Inertial Elements.

control inputs, the stability derivative matrix is [2]:

$$\begin{vmatrix} -ms + \frac{\partial X}{\partial \dot{x}} & \frac{\partial X}{\partial \theta} s - mg \\ \frac{\partial \theta}{\partial x} & -\mathrm{I}_{YY} s^2 + \frac{\partial \theta}{\partial \dot{\theta}} s \end{vmatrix} \begin{vmatrix} \dot{x} \\ \theta \end{vmatrix} = 0 \quad (26)$$

This uses the standard stability derivatives given in Prouty [Prouty, 2002, pp 564] – X is the longitudinal position, *theta* is the pitch angle and s is the Laplace transform of the differential operator. We modify the standard treatment of helicopters by multiplying $\partial M/\partial \dot{x}$, and $\partial X/\partial \dot{x}$ by 4 for the four rotors, as well as adding a term in $\partial\theta/\partial\dot{\theta}$ due to the vertical motion of the rotors in pitch and roll:

$$\frac{\partial \theta}{\partial \dot{\theta}} = \ldots - \rho A (\omega R)^2 2d \frac{\partial C_\mathrm{T}}{\partial \dot{\theta}} \quad (27)$$

where

$$\frac{\partial C_\mathrm{T}}{\partial \dot{\theta}} = \frac{-a}{8} \sigma \frac{1}{\omega R} \quad (28)$$

The characteristic equation of the system matrix determinant becomes:

$$s^3 - \left(\frac{1}{m} \frac{\partial X}{\partial \dot{x}} + \frac{1}{\mathrm{I}_{YY}} \frac{\partial \theta}{\partial \dot{\theta}} \right) s^2 + \frac{g}{\mathrm{I}_{YY}} \frac{\partial \theta}{\partial \dot{x}} = 0 \quad (29)$$

Solving for the roots of this polynomial gives the exponential components of the dynamic behaviour of the system. Since

$$\left(\frac{1}{m} \frac{\partial X}{\partial \dot{x}} + \frac{1}{\mathrm{I}_{YY}} \frac{\partial \theta}{\partial \dot{\theta}} \right) > 0 \quad (30)$$

and

$$\frac{g}{\mathrm{I}_{YY}} \frac{\partial \theta}{\partial \dot{x}} > 0 \quad (31)$$

for any system, it is clear that the unforced, open-loop dynamics can never be stable for the X-4.

Application of Routh's Discriminant, as outlined in Prouty, uses the characteristic polynomial to determine the nature of the instability. The Routh's Discriminant, $R.D.$, is given by

$$R.D. = AD - BC \quad (32)$$

where A, B, C and D are the coefficients of 29. If it is positive, the craft will exhibit pure divergence. If negative, the craft will exhibit unstable oscillation. If zero, the pitch dynamic will be neutral. In this case:

$$R.D. = -C_\mathrm{T} \rho A \left(\omega R\right)^2 h \quad (33)$$

Of the composing terms, only h can change signs. For a conventional helicopter, where $h < 0$, the craft has an unstable pole pair. If the rotors are inverted (above the CoG), the craft will diverge without oscillation. If the rotors and CoG are coplanar, the craft is marginally stable. This behaviour was demonstrated in a full 3D simulation previously [Pounds *et al*, 2004].

	Value	Error
p_1	$-2.507 + 2.671i$	$\pm 0.714 + 1.244i$
p_2	$-2.507 - 2.671i$	$\pm 0.714 + 1.244i$
p_3	2.578	± 1.129
z	-0.015	± 0.003

Table 4: Poles and Zeros of the Open Loop Pitch Dynamics.

4.3 Parameterised Model Envelope

Using the physical values for the flyer, the coupled pitch and ξ_X translational dynamical equations can be computed. The error range of the parameters maps the roots of the plant into a space on the complex plane. Linearised differential equations for the flyer are:

$$m\ddot{x} = -mga_{1_s} - mg\theta \quad (34)$$

$$\mathrm{I}_{YY}\ddot{\theta} = 4dC_\mathrm{T}\rho AR^2\omega_0\delta\omega + Ta_{1_s}h - \frac{a}{2}\sigma\rho AR\omega_0 d^2\dot{\theta} \quad (35)$$

These can be solved for a single transfer function $H = \Theta/\delta\omega$ between pitch angle, θ, and the input change in rotor speeds, $\delta\omega$:

$$\mathrm{H} = \frac{4dC_\mathrm{T}Rc_2(s+gc_1)}{(s+gc_1)(\mathrm{I}_{YY}s^2 - hmgc_3 s + \frac{a_0}{2}\sigma c_2 d^2 s) + hmg(gc_3 s - g))} \quad (36)$$

where

$$c_1 = \frac{4\theta_t - 2\lambda}{\omega R} \quad (37)$$

$$c_2 = \rho AR\omega_0 \quad (38)$$

$$c_3 = \frac{16}{\gamma\omega_0} \quad (39)$$

We approximate the flapping angle as a linear function of $\dot{x}$ and $\dot{\theta}$:

$$a_{1_s} = c_1\dot{x} + c_3\dot{\theta} \quad (40)$$

Using the previously given parameters and errors, the poles and zeros of the system are given in Table 4. The rotor height above the CoG is the largest contributor to error, producing more than 80 per cent of the error of each pole calculation. Thus, accurate knowledge of the rotor height is important to determining the dynamic model.

The unforced stability analysis demonstrated that h is also important in determining the behaviour of the dynamic system. The root locus for h shows that the structure of the open-loop poles changes significantly as h changes sign (cf. Fig. 5). Analogous to the unforced case, the system exhibits an unstable oscillation when

2. We use Prouty's aircraft coordinate notation in stability and control analysis for clarity

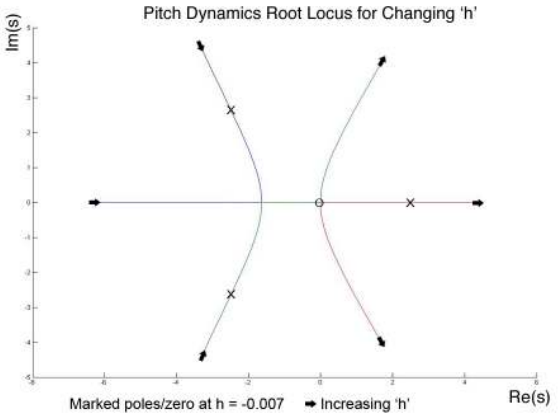

Figure 5: Root Locus of Pitch Dynamics for Changing Rotor Height Above CoG.

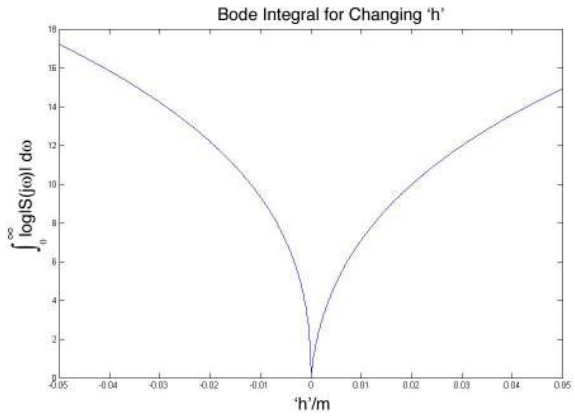

Figure 6: Bode Integral With Respect to Rotor Plane Placement.

the CoG is below the rotor, pure divergence when it is above the rotor, and neutral stability when coincident with the rotor.

Prouty suggests that helicopters can benefit from an inverted rotor configuration, as pure divergence is easier for a human pilot to correct for than unstable oscillation [Prouty, 2002, pp 603].

4.4 Design for Optimal Sensitivity

The use of automatic compensators no longer requires that a system be intuitive for a human pilot, and so oscillatory systems are acceptable. Instead, we use the fundamental limits of control to configure the plant for controller performance.

For good performance we want strong disturbance rejection and fast response to input commands. However, the 'Waterbed Effect' of the Bode integral for the sensitivity function imposes a limit on arbitrary design targets for the controller across all frequencies: it states that any arbitrary reduction in the sensitivity of the system implies a corresponding increase in sensitivity over other frequencies [Seron *et al*, 1997].

For this reason, it it desirable to reduce the Bode integral of the underlying system, prior to the application of any control. The Bode integral can be related directly to the poles of the open-loop plant. From Seron *et al*:

$$\int_0^\infty \log|S(e^{j\omega})|d\omega = \pi \sum_{i=1}^{n_p} p_i \qquad (41)$$

where S is the sensitivity function of the system, p_i are the poles of the open loop plant, and ω is frequency.

Calculating the Bode integral for a range of h from -0.05 to 0.05 m below the rotor demonstrates a sharp notch at $h = 0$ (cf. Fig. 6). When the rotor plane is coincident with the center of gravity, the bode integral is zero. In this configuration, the pitch dynamic is neutral.

The magnitude of the integral changes sharply as the rotor plane moves away from the CoG. Given the strong correlation between h error and plant model error, and the link between control sensitivity and h position, it is clear that close attention to the correct tuning and verification of rotor height is essential for the performance of the helicopter.

For the X-4 Flyer, the ideal rotor position is at $h = 0$. However, as the root locus with changing h demonstrates, the structure of the plant undergoes significant change with error around this point. For this reason, we set the CoG slightly away from the rotor plane so that small errors will not have an impact on stability. [3]

5 Control and Simulation

A variety of control techniques have been implemented successfully on quad-rotor UAVS – these include PID and LQ [Bouabdallah *et al*, 2004] and PD^2 [Tayebi and McGilvray, 2004] control. Bouabdalla found that PID performed favourably compared to LQ due to the simpler method's tolerance for model uncertainty. This quality is desirable for our full flapping model which is especially sensitive to changes in h.

In addition to the attitude dynamics, the X-4 Flyer also has important motor dynamics. The motor dynamics act in series with the rigid body dynamics – fast motor response is important for authoritive attitude control of quad-rotors. To this end, rotor speed controllers have been developed to improve the natural performance of the rotor-motor system [Pounds *et al*, 2007]. The linearised closed-loop motor system transfer function, $H_{\text{M-CL}}$, is:

$$H_{\text{M-CL}} = \frac{68.85(s + 0.42)}{(s + 78.46)(s + 0.44)} \qquad (42)$$

3. In practice, the X-4's rotors are set slightly above the CoG at $h = -0.07$ m so it may be optionally piloted by a human.

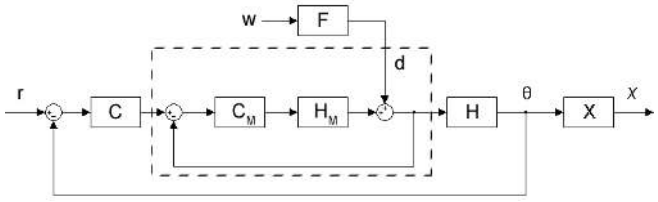

Figure 7: Disturbance Propagation Block Diagram.

where u is the input reference speed.

5.1 Discretised Model

The controller runs at 50 Hz, the maximum frequency at which attitude data is updated, and so the dynamics of the plant are discretised at $t_s = 0.02$ seconds for the control design. The IMU returns both angle and rate information, which allows for an improper PID controller to be realised. The complete discretised model, $G_c = \theta/\delta u$, is:

$$\mathrm{G_c} = \frac{1.4343\times10^{-5}(z-0.9916)(z+1)(z-0.9997)}{(z-0.2082)(z-0.9914)(z-1.038)(z^2-1.943z+0.9448)} \quad (43)$$

where δu is the differential variation in rotor speed about the operating condition, 850 rad·s^{-1}. The additional zero at $z = -1$ comes from the matched pole-zero discretisation method.

5.2 Controller Design

The proposed controller consists of a pure integrator for zero angle tracking error and a complex zero pair to stabilise the plant. The transfer function of the controller, C, is:

$$C = \frac{2210(z^2 + 1.9z + 0.9045)}{z - 1} \quad (44)$$

As the motor dynamics are so fast, the dominant pole has little interaction with the attitude mechanics. If it were slower, the excess poles would diverge closer to the unit circle, leading to oscillation and possibly instability. The slow motor pole-zero cancellation is associated with the dynamics of the lithium ion polymer cells used to power the flyer. Sufficient gain causes the pole to close with the zero, reducing the influence of the effect.

5.3 Disturbance Rejection

The disturbances experienced by the attitude dynamics are expected to take the form of aerodynamic effects propagated through variations in the the rotor speed. We use the sensitivity model developed for the motor speed controller to predict the displacement in position due to a motor speed output disturbance (cf. Fig. 7). We desire to keep the X-4 Flyer position variation small, in the order of 0.5 m.

The rotor speed noise is modelled by an output disturbance to the rotor speed, d, characterised as white noise, w, passed through a coloured filter, F [Pounds *et al*, 2005] :

$$F = \frac{0.0143(s + 7)}{(s + 0.1)} \quad (45)$$

The pitch angle sensitivity due to w is given by:

$$\frac{\Theta}{W} = \frac{H}{1 + C_\mathrm{M}H_\mathrm{M}} \frac{C_\mathrm{M}H_\mathrm{M}}{C_\mathrm{M}H_\mathrm{M} + CH(1 + C_\mathrm{M}H_\mathrm{M})} F \quad (46)$$

where H_M is the motor plant and C_M is the motor compensator. The peak sensitivity in pitch angle is at 0.4 rad·s^{-1} (cf. Fig. 8).

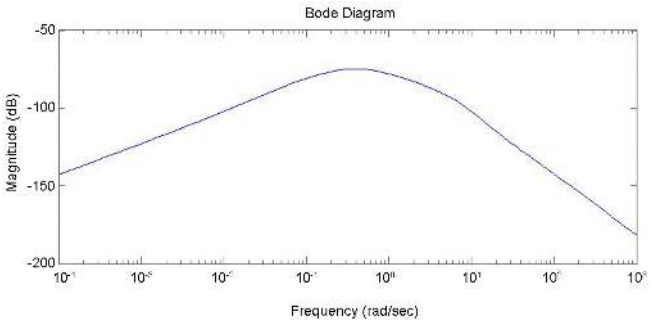

Figure 8: Pitch Angle Sensitivity Function Bode Plot.

Pitch angle is integrated to x position. Using equations 35 and 40, the transfer function, X, is:

$$X = \frac{-gc_3 - g}{s(s + gc_1)} \quad (47)$$

A unit disturbance at the peak angle sensitivity frequency yields a positional variation of 0.01 m, well within the target. However, due to the integral position dynamics, the peak sensitivity in x occurs at low frequencies to DC ($\omega_\mathrm{d} < 0.01$ rad·s^{-1}) at -6.3 dB; a unit sinusoid in this range will produce a corresponding position deviation of 0.78 m with negligible angle deviation. Note that this deviation is very slow – a period of 600 s – and would be easily compensated for, given position measurement.

5.4 Simulation

A complete simulation of the attitude control system was coded in Matlab Simulink. This included nonlinearities in the system arising from multiple sample times in the microcontrollers, saturation of the motors, quantisation of measurements and slew limitation in the motor controller.

In simulation, the closed loop system has a unit impulse response settling-time of 2 seconds and 0.2 rad maximum anglular displacement. A unit sinusoid disturbance applied at $w = 0.01$ rad·s^{-1} produced small angular displacements that were subsumed by the small nonlinear effects of the model and did not propagate into

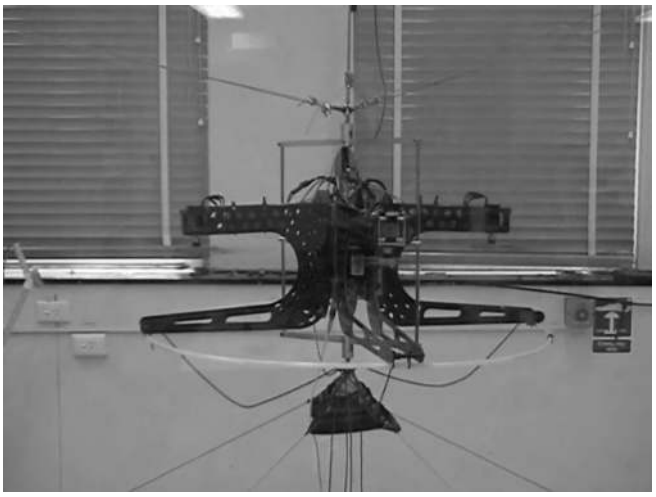

Figure 9: X-4 Flyer Stabilised in Pitch and Roll.

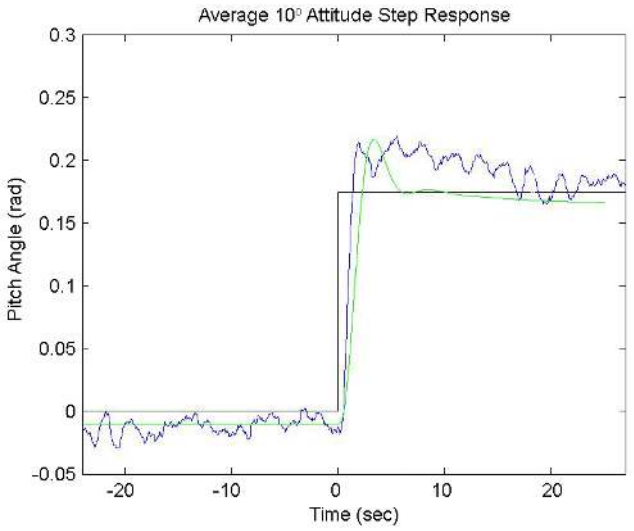

Figure 10: Low Speed Average Step Reference (black), Data (blue) and Prediction (green).

the output. It is likely that error measurements due to slow disturbance effects will be lost in the quantisation of the sensor readings.

6 Implementation and Performance

Prior to the designed controller being tested under flight conditions, we tested the controller on a tether apparatus. In this configuration, no flapping occurs due to horizontal motion since the flyer is fixed in space, free only to rotate in pitch and roll. In practice, it was found that the tethered X-4 exhibits two additional stable oscillatory poles at $z = 0.9664 \pm 0.0331$, from mechanical cross-coupling with the test rig. The rotors can be operated at reduced speeds to conserve battery power during initial testing – at these speeds, the system gain changes in proportion to the rotor speed. The resultant simplified full-speed system transfer function becomes:

$$G_{\text{rig}} = \frac{1.87 \times 10^{-8}(z+1)^3}{(z-1.0)(z-0.953)(z^2-1.933z+0.935)} \quad (48)$$

This requires modification to the controller to place the zeros on the real axis:

$$C_{\text{noflap}} = \frac{2210(z^2+1.9z+0.9)}{z-1} \quad (49)$$

When implemented, it was found that the controller worked reliably for low rotor speeds ($\omega < 450$ rads^{-1}). The X-4 can stabilise itself in pitch and roll, and remain within 2 degrees of level (cf. Fig. 9). To test the dynamic performance, twenty-two step experiments were performed over 800 seconds, from which steps were averaged for analysis (cf. Fig. 10). The step motion was alternating 10 degrees pitch forwards and backwards from level, to eliminate directional bias. Roll was held at 0 degrees by the controller and yaw was locked in place on the test rig.

From the data, the system has a 1.25 second rise-time, 30 per cent overshoot and a slow 40 second settling time, compared with the 2.15 second rise-time, 30 per cent overshoot and 15 second settling time the model predicts at this rotor speed. The step clearly shows the influence of the two test-rig poles producing a 0.4 Hz oscillation with ± 1 degree angular variation. This oscillation would lead to horizontal displacement of ± 0.027 m, were the X-4 in flight.

It was found that as the rotor speed increases, the system displays chaotic semi-stable behaviour that would make untethered flight impossible. We believe that the instability is due to high-frequency noise from the rotors destroying the validity of IMU accelerometer data. We are confident that additional isolation of the sensors will allow full-speed operation.

7 Conclusion

We have developed a larger quad-rotor platform than is typically used in current robotics research. The analysis of flyer attitude dynamics allowed us to tune the mechanical design for best control sensitivity and disturbance rejection. We designed a controller to stabilise the dominant decoupled pitch and roll modes, and use a model of disturbance inputs to estimate the performance of the plant. It was found that the compensator sucessfully regulates attitude at low rotor speeds.

8 Acknowledgements

The authors would like to thank CSIRO ICT Robotics for its ongoing support of this project.

References

[Bouabdallah *et al*, 2004] S. Bouabdallah, A. Noth and R. Siegwart. PID vs LQ Control Techniques Applied to an Indoor Micro Quadrotor. In *Proceedings of the IEEE International Conference on Intelligent Robots and Systems*, Sendai, Japan, 2004.

[Guenard *et al*, 2005] N. Guenard, T. Hamel and V. Moreau. Dynamic Modeling and Intuitive Control Strategy for an "X4-Flyer". In proceedings of *5th International Conference on Control and Automation*, Budapest Hungary, June, 2005.

[Hamel *et al*, 2002] T. Hamel, R. Mahony, R. Lozano and J. Ostrowski. Dynamic Modelling and Configuration Stabilization for an X4-Flyer. In proceedings of *15th Triennial World Congress of the International Federation of Automatic Control*, Barcelona, July, 2002.

[Leishman, 2006] J. G. Leishman. Principles of Helicopter Aerodynamics, 2nd Ed. Cambridge University Press, Cambridge, United Kingdom, 2006.

[Pounds *et al*, 2004] P. Pounds, R. Mahony, J. Gresham, P. Corke and J. Roberts. *Towards Dynamically-Favourable Quad-Rotor Aerial Robots.* In *Proc. of Australasian Conference on Robotics and Automation*, Canberra, Australia, 2004.

[Pounds *et al*, 2005] P. Pounds, R. Mahony and P. Corke. *Small-Scale Aeroelastic Rotor Simulation, Design and Fabrication.* In *Proc. of Australasian Conference on Robotics and Automation*, Sydney, Australia, 2005.

[Pounds *et al*, 2007] P. Pounds, R. Mahony and P. Corke. *System Identification and Control of an Aerobot Drive System.* In *Proc. of Information, Decision and Control*, Adelaide, Australia, 2007, *submitted.*

[Prouty, 2002] R. W. Prouty. Helicopter Performance, Stability, and Control. Krieger Publishing Company, 2002, reprint with additions, original edition 1986.

[Seron *et al*, 1997] M. M. Seron, J. H. Braslavsky and G. C. Goodwin. Fundemental Limitations in Filtering and Control. Springer-Verlag, London, United Kingdom, 1997.

[Tayebi and McGilvray, 2004]
A. Tayebi and S. McGilvray. *Attitude Stabilization of a Four-Rotor Aerial Robot.* In proceedings of *43rd IEEE Conference on Decision and Control*, Atlantis, Paradise Island, Bahamas, pp14-17, December, 2004.